
Macro2Micro: Cross-modal Magnetic Resonance Imaging Synthesis Leveraging Multi-scale Brain Structures

Sooyoung Kim*
Seoul National University

Joonwoo Kwon*
Seoul National University

Junbeom Kwon*
Seoul National University

Sangyoon Bae
Seoul National University

Yuwei Lin
Brookhaven National Lab

Shinjae Yoo[†]
Brookhaven National Lab

Jiook Cha[†]
Seoul National University
connectome@snu.ac.kr

Abstract

Spanning multiple scales—from macroscopic anatomy down to intricate microscopic architecture—the human brain exemplifies a complex system that demands integrated approaches to fully understand its complexity. Yet, mapping nonlinear relationships between these scales remains challenging due to technical limitations and the high cost of multimodal Magnetic Resonance Imaging (MRI) acquisition. Here, we introduce **Macro2Micro**, a deep learning framework that predicts brain microstructure from macrostructure using a Generative Adversarial Network (GAN). Grounded in the scale-free, self-similar nature of brain organization—where microscale information can be inferred from macroscale patterns—Macro2Micro explicitly encodes multiscale brain representations into distinct processing branches. To further enhance image fidelity and suppress artifacts, we propose a simple yet effective auxiliary discriminator and learning objective. Our results show that Macro2Micro faithfully translates T1-weighted MRIs into corresponding Fractional Anisotropy (FA) images, achieving a 6.8% improvement in the Structural Similarity Index Measure (SSIM) compared to previous methods, while preserving the individual neurobiological characteristics.

1 Introduction

The brain is a complex multi-scale system, with its structure and function emerging from interactions at the molecular, cellular, circuit, and network levels [14]. This hierarchical organization, ranging from microscopic cellular components to macroscopic anatomical characteristics, underlies the dynamic functionality of the brain [42, 5, 14, 11, 30, 4, 47, 3, 49]. The intricate organization across multiple scales is essential for the brain’s dynamic functionality, yet comprehending this organization remains a significant challenge [12]. Advances in Magnetic Resonance Imaging (MRI) now allow simultaneous exploration of both large-scale anatomy and fine-grained tissue properties, offering unprecedented opportunities to investigate brain structure-function relationships across scales.

*These authors contributed equally to this work.

[†]Co-corresponding author.

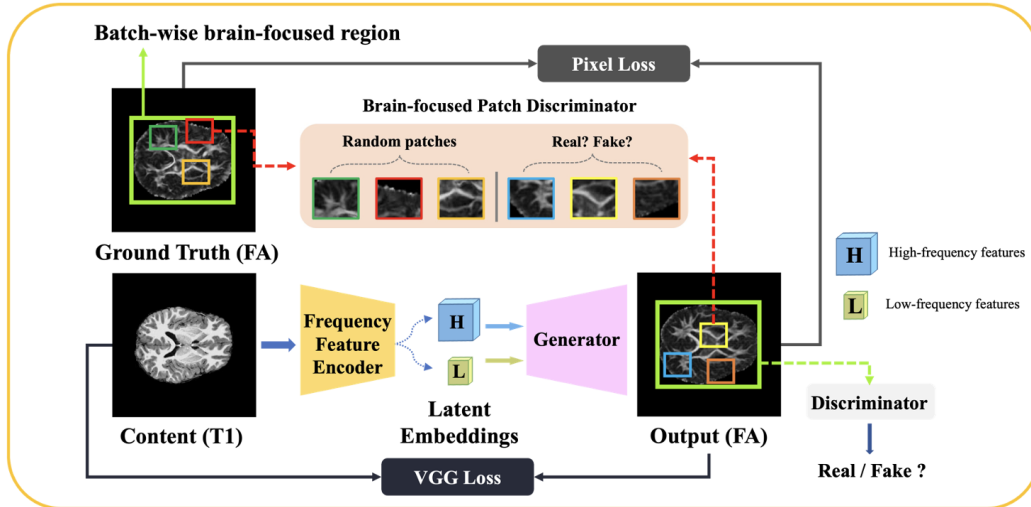


Figure 1: The overall architecture of the proposed model.

At the macroscopic level, structural MRI (sMRI), such as T1-weighted imaging, captures the brain’s macrostructure, which includes gray matter cell bodies, neurites, white matter axonal arrangements with myelin content, cerebrospinal fluid (CSF), fat, and inflammation. Understanding this macrostructure provides critical insights into the brain’s organization and its abnormalities, including lesions [15] and neurodegenerative diseases [21, 13]. Diffusion Tensor Image (DTI) provides insight into the brain’s microstructure by measuring water diffusion patterns that reflect axonal density, fiber orientation, and microstructural integrity [17, 39]. These microscopic features play an essential role in identifying tissue damage [27], psychiatric disorders such as schizophrenia [28] and depression [38], and neurological diseases such as Alzheimer’s dementia [10, 32] and Parkinson’s disease [50, 35]. Integrating both macro- and microstructural information is thus essential for a comprehensive understanding of the brain’s connectivity and function [11, 30].

However, acquiring high-quality multimodal MRI data is resource-intensive and time-consuming. T1-weighted MRI requires a single scan, whereas DTI demands multiple scans—at least six for accuracy and up to thirty for rotational invariance [24, 25]. Simultaneous acquisition of high-quality MRI modalities is often impractical due to lengthy scanning times, which can induce patient discomfort, especially in those with panic disorders [31, 33], and may result in motion artifacts [41, 46]. These limitations have spurred efforts to develop methods for generating high-quality DTI from fewer scans [45], but challenges persist.

T1-weighted sMRI data, characterizing mainly macrostructure, have been shown to carry information that can approximate microstructural features of white matter [20, 18, 1, 2]. This indicates that microstructural estimates—akin to those obtained via DTI—could be inferred from macrostructural MRI scans, potentially circumventing the need for lengthy, multimodal acquisitions. Emerging deep learning methods present a promising pathway toward cross-modal MRI synthesis [48, 43, 40, 7]. Building on earlier successes in macro-to-micro translation [18, 1, 2], there is an opportunity to improve synthesis quality, better preserve individual biological characteristics, and achieve accurate and efficient cross-modal data generation. Such advances can expand access to multimodal MRI biomarkers, accelerating both clinical diagnostics and fundamental neuroscience research.

To address these challenges, we introduce **Macro2Micro**, a novel image-to-image translation framework for cross-MRI modality synthesis. Grounded in the principle that macroscale anatomical features can inform microscale structures, Macro2Micro employs a Generative Adversarial Network (GAN) [16] to disentangle and encode multiscale brain representations into distinct processing streams. This architecture enables active information exchange between high- and low-frequency branches, enhancing its ability to capture structural connectivity across modalities.

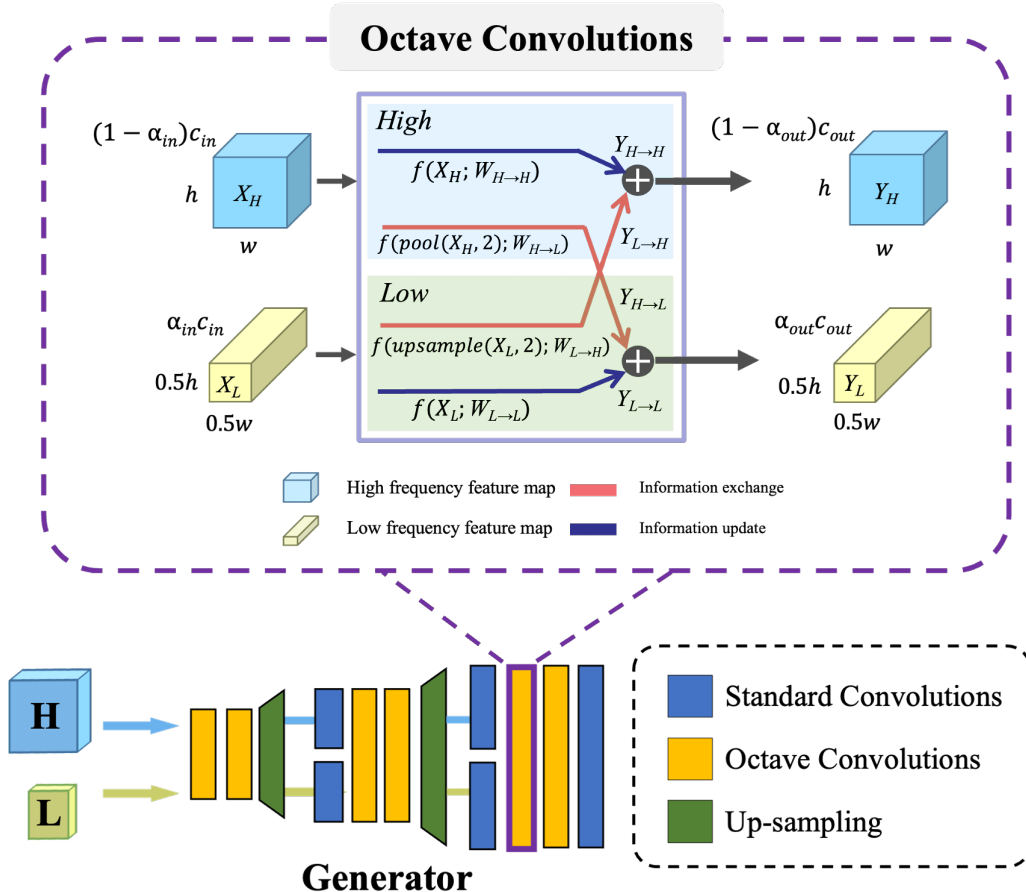


Figure 2: The structure of Octave Convolutions (Top) and the generator design (Bottom). H and L represent High- and Low-frequency features respectively.

2 Method

Fig. 1 gives an overview of our framework for cross-modal MRI synthesis. The subsequent sections include an exhaustive analysis of the proposed method and its underlying principles.

Architecture Overview. The proposed architecture consists of four components: a frequency feature encoder E , a generator G , a discriminator D , and a brain-focused patch discriminator $D_{brainPD}$. Specifically, the input MR images are decomposed into two distinct frequency feature maps through a frequency feature encoder E , encoding information on the macro-structure of the brain into low-frequency components and information on the microstructure of the brain into the high-frequency components. These encoded latent features are subsequently fed to the generator, where the synthesized high and low-frequency outputs of the target modality are made from the input latent features. The terminal layer of the generator combines the synthesized high and low-frequency outputs to generate the final output. This output are then fed to both the discriminator D and the brain-focused patch discriminator $D_{brainPD}$. These two discriminators guide our model to effectively synthesize target modality by focusing on the delicate details in the brain region in the input and learning the statistical relationships between each image patch.

Octave Convolutions. One of the key elements of the proposed model is utilizing Octave Convolutions (OctConv) [8] to encode macro- and micro-scale information into the corresponding frequency feature maps. To factorize input mixed feature maps based on their frequencies, the spatial resolution of low-frequency feature maps in OctConv is decreased by one octave, where the term *octave* refers to a spatial reduction divided by a power of two. In this study, a value of 2 was chosen for simplicity. The spatial reduction in the low-frequency branch expands the receptive field of the low-frequency

processing branch, capturing more contextual information from distant locations and improving synthesis performance. Following the convention presented by previous research, AesFA [29], the up-sampling order is modified to effectively address checkerboard artifacts [34]. The detailed design of OctConv used in this study is illustrated in Fig. 2. Here, the α value refers to the ratio of the low-frequency channels to high-frequency channels, and empirical findings indicate that employing OctConv with half the channels for each frequency ($\alpha = 0.5$) yields optimal performance. A comprehensive experiment regarding this matter can be found in the section 3.

Frequency Feature Networks. Both the frequency feature encoder and the generator are equipped with several layers of OctConvs. This idea was originated from the previous study [29]. However, our work differs from theirs in that we primarily focus on encoding different scales of information from the brain into the corresponding frequency components without any auxiliary encoder. While latent features decomposed by the encoder are convolved in the generator, the two frequency features actively exchange information with the opponent via information exchange branches. This active information exchange between frequency components compensates for the missing information in each branch and boosts the entire synthesis process. The standard convolutions after up-sampling operations are responsible for learning frequency-agnostic information and compensating for the missing information during up-sampling operations. The effectiveness of active information exchange is outlined in the section 3.

Brain-focused Patch Discriminator. While using the discriminator solely seems sufficient for synthesizing the target modality, the results still suffer from the checkerboard artifacts and undesired artifacts (see the section 3 for the details). To tackle this, we employed a patch co-occurrence discriminator, introduced by [36]. We encourage patches cropped from the output to maintain the identical representation as the patches cropped from the target MR images. Consequently, the generator aims to generate an output image such that any patch from the output cannot be distinguished from a group of patches from the actual MR images.

However, most brain Magnetic Resonance Images contain extensive background regions. These regions are primarily zero-values or noises. Cropping patches from such regions and feeding them to the discriminator are inefficient and could lead to the degradation of output image quality (e.g., blurring or dimmer images and pixelization) as the model would learn the background noises or the abrupt changes in the boundary of our brain and the background. To effectively cope with this, we applied a simple yet effective pre-processing algorithm. We first calculate the valid brain regions in the training mini-batch, which are then used to crop the valid region from the given training mini-batch. By doing so, our brain-focused patch discriminator serves to focus on the effective regions of the brain and enforce that the joint statistics of a learned representation consistently follow the ground truth modality.

Learning Objectives. To guide our model to learn subject-independent representation and the connectivity between the macro and micro-structure of the human brain while synthesizing the target modality with desired image quality, we use the mean square error (\mathcal{L}_{pix}) between the output I_{out} and ground truth I_{GT} and the discriminator objectives (\mathcal{L}_{GAN}):

$$\mathcal{L}_{\text{pix}} = \|I_{\text{out}} - I_{\text{GT}}\|_1, \quad \mathcal{L}_{\text{GAN}} = \mathbb{E}[-\log(D(I_{\text{out}}))]$$

For the brain-focused patch discriminator, we follow the loss of Swap-AE [36], but with slight changes described in the previous section. The final GAN loss for the brain-focused patch discriminator is as follows:

$$\mathcal{L}_{\text{patch}} = \mathbb{E}[-\log(D_{\text{patch}}(\text{crops}(\text{valid}(I_{\text{out}})), \text{crops}(\text{valid}(I_{\text{GT}}))))]$$

where *crops* operator selects a random patch of size 1/2 to 1/3 of the full image dimension on each side and *valid* operator calculates the valid brain regions in the given training mini-batch and then crops according to them.

To prevent the model from falling the mode-collapse and generating skull-like artifacts (see the details in Fig. 6), we utilize prior knowledge from a pre-trained convolutional neural network, such as VGG-19 [44]. The perceptual loss was originally proposed by [23], yet has not been actively addressed in the Magnetic Resonance Imaging domain to cope with the mode collapse. The perceptual objective we used is as follows:

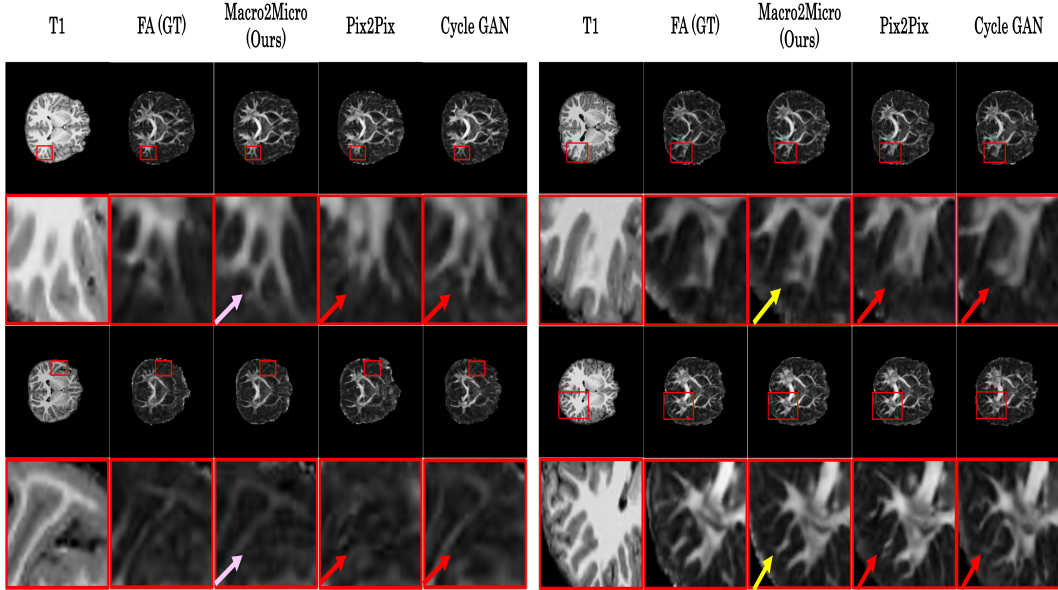


Figure 3: Qualitative Comparison of images made with our proposed model (Macro2Micro), and images made with Pix2Pix and CycleGAN. Magnify the image to see the details.

$$\mathcal{L}_{\text{perct}} = \sum_{n=1}^4 \|f_n(I_{\text{out}}) - f_n(I_{\text{GT}})\|_2$$

where f_n symbolizes the n -th layer in the VGG-19 model. The perceptual loss is computed at the $\{\text{conv1}_1, \text{conv2}_1, \text{conv3}_1, \text{conv4}_1\}$. Considering all the aforementioned losses, the total loss is formalized as:

$$\mathcal{L}_{\text{total}} = \lambda_{\text{pix}}\mathcal{L}_{\text{pix}} + \lambda_{\text{perct}}\mathcal{L}_{\text{perct}} + \lambda_{\text{GAN}}\mathcal{L}_{\text{GAN}} + \lambda_{\text{patch}}\mathcal{L}_{\text{patch}}$$

where λ_{pix} , λ_{perct} , λ_{GAN} , and λ_{patch} are the weighting hyper-parameters for each loss.

Experimental Settings and Data. To demonstrate the effectiveness of the proposed model, we synthesized DTI from sMRI (Fig.1). Specifically, T1-weighted images were used for sMRI, and Fractional Anisotropy (FA) images were used to represent DTI. The Adolescent Brain Cognitive Development (ABCD) dataset [6] was utilized for this study, which includes comprehensive developmental data and structural brain MRI collected from children across multiple sites in the United States. Detailed descriptions of the image acquisition protocol and the minimal processing pipeline can be found in previous studies [6, 19].

For the image-to-image translation task, we used T1-weighted images and corresponding FA images with dimensions of $256 \times 256 \times 256$ and a voxel size of 1mm. A total of 7,669 quality-controlled subjects from the ABCD dataset were included in the analysis.

Implementation Details. During training, all images are loaded as 256x256 pixels and scaled to [0, 1]. The model is trained using the Adam optimizer [26] with a learning rate 0.0002 and a batch size of 8 for 200 epochs. The encoder feature map has dimensions of (128, 64, 64) for high and (128, 32, 32) for low-frequency components. The baseline models outlined in this paper were trained using the author-released codes and parameters. Baselines and all our experiments are conducted using the PyTorch framework [37] on a single NVIDIA RTX A5000(24G) GPU.

3 Experimental Results

Diffusion Tensor Image Synthesis. We compared our Macro2Micro model with existing image translation models (i.e., Pix2Pix [22] and CycleGAN [51]) (Fig. 3). Our model could faithfully reconstruct the structural location and FA value with minimum residuals while maintaining both

Table 1: Quantitative comparison with generated whole brain FA (FA) images and white matter (WM) whose FA value is bigger than 0.2 from synthesis outputs. The best outcomes are shown in **bold**. \uparrow : Higher is better. \downarrow : Lower is better.

Methods	Input (GT)	SSIM (\uparrow)	PSNR (\uparrow)	MAE (\downarrow)	MSE(\downarrow)
Pix2Pix	FA	0.8310	24.7738	0.1469	0.1292
CycleGAN	FA	0.8332	24.6660	0.1477	0.1299
Macro2Micro (Ours)	FA	0.8600	25.7560	0.1383	0.1226
Pix2Pix	WM	0.8354	24.8992	0.1374	0.1200
CycleGAN	WM	0.8369	24.7585	0.1383	0.1208
Macro2Micro (Ours)	WM	0.8627	25.8493	0.1300	0.1146

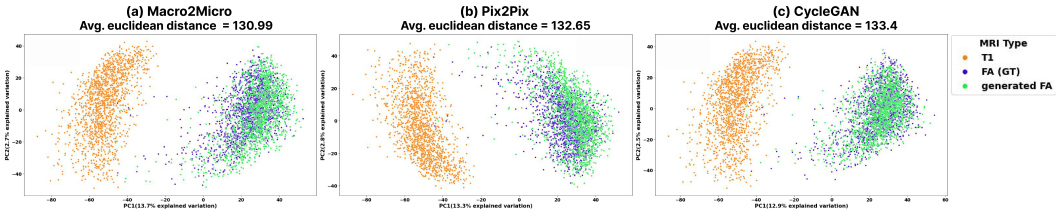


Figure 4: PCA results for the T1, FA (Ground Truth), and generated FA images from (a) Micro2Macro, (b) Pix2Pix, and (c) CycleGAN. The Euclidian distance below each model name indicates the average distance between the FA (Ground Truth) and the generated FA images.

isotropic and anisotropic movement of water molecules in the given brain. In terms of white matter and overall brain structure, all models translate target modality with comparable quality. However, Pix2Pix and CycleGAN could not recognize and synthesize intricate micro-scale structures in many cases. For instance, results from baseline models mostly neglected and underexpressed the microscopic white matter at the boundaries of the brain (red arrows), whereas our model does not (green arrows). Owing to its ability to learn both macro- and microstructures from both modalities, our model not only generates the most comparable images to the ground truths but also captures structural details lost in the original and reconstructs parts that were previously disconnected or absent. For example, our model learns the presence of the white matter from FA image while determining its morphology from the T1 image (pink and yellow arrows and their corresponding T1 and FA). Similarly, our model shows better quality by bending the straight white matter line in ground truth to its more specific endpoint (yellow arrows) by referencing the macro-structure from the T1 image. In terms of quantitative comparisons, Macro2Micro shows the best performance, achieving the best SSIM, PSNR, MAE, and MSE (Table 1). In addition, this result holds even when we compared the results within the white matter regions (voxels with FA greater than 0.2).

To further test the robustness and effectiveness of the proposed model, we conducted principal component analysis (PCA) on three types of images: T1-weighted images, ground truth FA images, and synthesized FA images. We analyzed and visualized 1,499 subjects in the test dataset. After flattening 256^2 voxels from MRI slices, we removed the non-brain background, leaving 26,891 voxels for each brain modality, PCA was then applied to the entire features. A batch size of 200 was utilized for the incremental PCA and the visualization was performed using two principal components. The two principal components individually accounted for 13.7% and 2.7% of the variances. Notably, the PCA result demonstrated that the generated FA images exhibited significant dissimilarity compared to the original T1 images while displaying an overlap with the ground truth FA images in the low-dimensional representation (Fig. 4).

Prediction of Biological and Cognitive Variables. The image-to-image translation approach is powerful in terms of image transformation; however, there may be a major concern about potential damage to biological characteristics [9]. To test whether biological information from the brain images is preserved during the translation process, we conducted a task of predicting the sex, intelligence, and Attention-Deficit/Hyperactivity Disorder (ADHD) diagnosis of children using both predicted and ground truth FA images. Implementation details for these downstream tasks are in supplementary materials. We present the performance of the generalized linear model (GLM) on sex, intelligence, and ADHD prediction tasks in Table 2. It is worth noting that Macro2Micro yielded an AUROC of 0.782 in the sex classification, slightly higher than that of ground-truth FA images (0.7641) and

Table 2: ADHD, Sex classification and Intelligence regression performance of real T1, real FA, and synthesized FA images.

Input	ADHD		Sex		Intelligence	
	AUROC (\uparrow)	ACC (\uparrow)	AUROC (\uparrow)	ACC (\uparrow)	Corr.Coeff. (\uparrow)	MSE (\downarrow)
T1	0.5034	0.5479	0.7820	0.7133	0.159	0.777
FA (GT)	0.4812	0.5342	0.7641	0.7066	0.124	0.832
FA (Pix2Pix)	0.5532	0.5821	0.7565	0.6800	0.187	0.784
FA (CycleGAN)	0.4445	0.4794	0.7534	0.6766	0.066	0.836
FA (Macro2Micro)	0.4926	0.5136	0.7726	0.6866	0.166	0.797

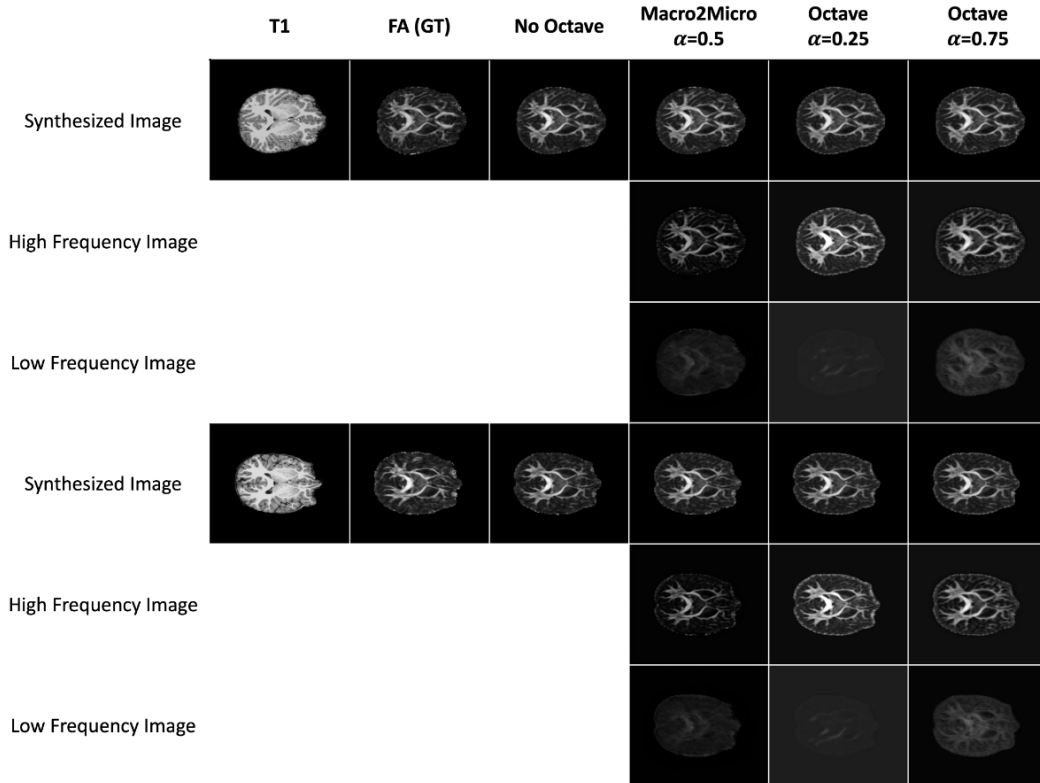


Figure 5: **Ablation study** Qualitative comparison of the effectiveness of Octave Convolution.

other algorithms. Although Pix2Pix showed the best performance in predicting ADHD diagnosis and intelligence, our model exhibited comparable performance for predicting ADHD diagnosis to ground truth FA images in terms of AUROC and surpassed the ground truth FA in predicting Intelligence. This suggests that the biological characteristics of different individuals could be preserved.

Effectiveness of Octave Convolution. We tested how Octave Convolution influences our suggested model. When Octave Convolution was utilized, both the SSIM and the PSNR improved, as demonstrated in Table 3. The α value in Octave Convolution represents the percentage of low-frequency features relative to total features and verifies the difference. In Figure 5, at an α of 0.25, it is clear that the low-frequency image has a low image contrast, while the high-frequency image has a high contrast. Low-frequency images reveal more information with an α of 0.75 than at values of 0.5 and 0.25. On the other hand, if α is set to 0.5, it's clear that the image-based separation of high and low frequencies seems balanced. The best results in terms of MAE, MSE, and inference time were achieved with an α value of 0.5, while an α value of 0.25 yielded the higher SSIM and PSNR but achieved similar image quality with an α value of 0.5 (Table 3).

Ablation Studies. Fig. 6 and Table. 3 show the effectiveness of design choices employed in our model. For brain-focused patch discriminator (brainPD), a model without brainPD generates artifacts

Table 3: Effects of brain-focused patch discriminator, the utilization of perceptual loss with a pre-trained VGG network, and a detailed inspection of the effect of Octave Convolutions and its low-frequency ratio (α).

Methods	SSIM (\uparrow)	PSNR (\uparrow)	MAE (\downarrow)	MSE (\downarrow)	Time (\downarrow)
Macro2Micro (w/o brainPD)	0.8663	26.2560	0.1440	0.1288	0.0110
Macro2Micro (w/o percept.loss)	0.8565	25.7207	0.1407	0.1251	0.0110
Macro2Micro	0.8631	26.0478	0.1374	0.1221	0.0110
No Octave	0.8598	25.8797	0.1280	0.1122	0.0056
Octave $\alpha = 0.25$	0.8640	26.1565	0.1417	0.1264	0.0126
Octave $\alpha = 0.50$ (Default)	0.8631	26.0478	0.1374	0.1221	0.0110
Octave $\alpha = 0.75$	0.8597	25.9887	0.1414	0.1258	0.0129

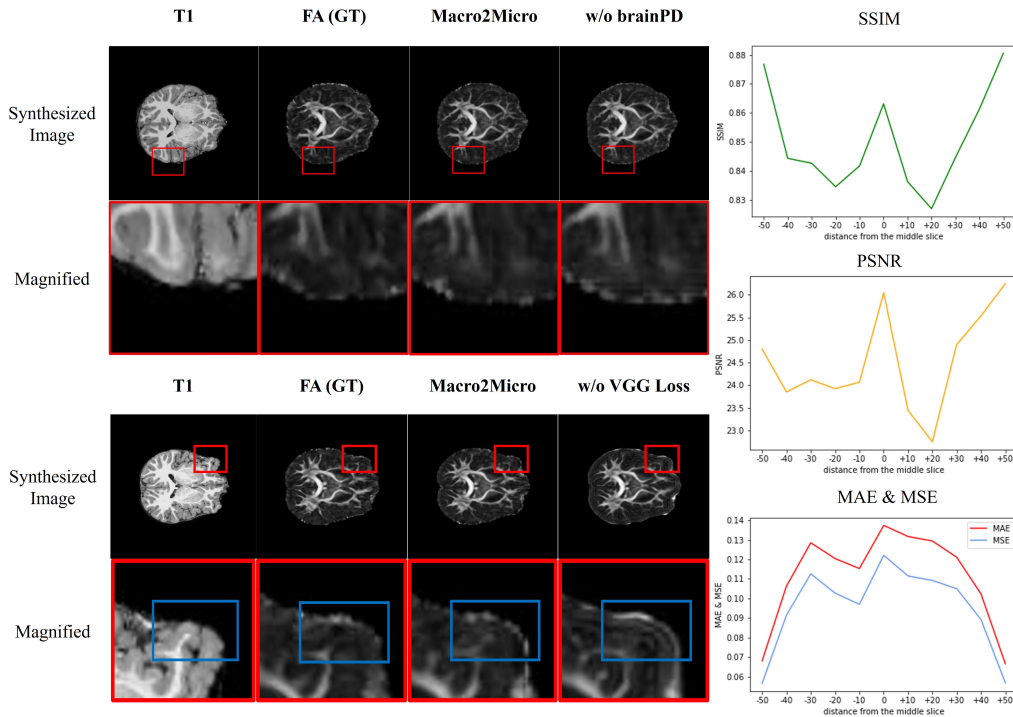


Figure 6: (Left) Generated FA images with and without using a brain-focused patch discriminator and perceptual loss using a pre-trained VGG network. (Right) Inference performance of our model along the distance from the center of the brain.

like white dots along the boundaries of the brain, and the checkerboard patterns are generated. As the brainPD focuses on the effective regions of the brain, the model with brainPD synthesizes the target modality in higher image quality with more delicate details and generates fewer artifacts. Similarly, a model trained without perceptual loss using a pre-trained VGG network shows lower performance in all evaluation metrics, generating severe artifacts that look like a brain skull at the boundary of the brain (blue rectangles).

Although our method was trained using only the central slice of the brain, it worked well not only in the center but also in its periphery. Figure 6 depicts how each evaluation metric shifts from the center to its periphery. Our model performs strongly in both the peripheral and central slices, showcasing its exceptional generability. It is worth noting that the score is higher towards the extreme end of the brain than in the center. We believe this is because the brain size in the image itself in the extreme end of the brain is smaller compared to the central slice. Therefore, the metric includes more backgrounds, resulting in improved performance.

4 Discussion

This work introduces Macro2Micro, a novel image-to-image translation framework that leverages a generative adversarial network (GAN) to infer microstructural brain features from macroscale MRI data. By integrating octave convolutions [8] for the first time in this context, Macro2Micro processes distinct frequency components of MRIs, enabling the model to effectively capture and synthesize complex, multiscale structural relationships. This design allows the model to disentangle relevant spatial information and facilitates active information exchange between frequency branches, resulting in more accurate representations of the brain’s structural connectivity.

Quantitative evaluations confirm that Macro2Micro outperforms widely used image-to-image translation models, such as CycleGAN [51] and Pix2Pix [22]. Beyond aligning closely with ground truth FA data, Macro2Micro sometimes generates more coherent white matter structures by inferring subtle microstructural patterns hinted at by T1-weighted scans but less evident in the original diffusion data. Principal component analysis (PCA) further supports these findings, showing that the generated FA images align closely with the distribution of real FA images, thereby enhancing the interpretability of the results. Crucially, the model also preserves important biological signals, as evidenced by its predictive accuracy for individual-level variables such as sex, intelligence, and ADHD diagnosis. Such robustness underscores Macro2Micro’s clinical and research relevance, laying a foundation for its integration into practical workflows.

Macro2Micro also addresses the challenge of redundant background regions in brain MRIs—a common source of noise and artifacts. By incorporating a brain-focused patch discriminator and cropping images into meaningful patches, the model emphasizes relevant brain regions, improving accuracy and reducing artifacts. Leveraging pre-trained convolutional neural networks, such as VGG-19 [44], Macro2Micro further refines anatomical details, sharpens boundaries, and minimizes distortions, including skull-like artifacts at the brain’s periphery.

While the model demonstrates significant promise, our study has several limitations. First, training the model on a single central slice restricts its generalizability to peripheral brain regions, where background predominates. Addressing this may require training on full brain volumes or incorporating additional learning objectives. Second, the model currently uses T1-weighted input and a single diffusion metric (Fractional Anisotropy), which limits the scope of microstructural features captured. Expanding to other MRI modalities and diffusion metrics could provide a more comprehensive understanding of brain microstructure. Third, the training data originates from a single study, raising concerns about generalizability to diverse imaging protocols, scanners, or populations. Future work should validate Macro2Micro across heterogeneous datasets and incorporate multi-contrast training to improve robustness and clinical applicability.

In summary, Macro2Micro takes a meaningful step toward bridging macro- and micro-scale brain analyses. By delivering biologically faithful, high-quality multimodal MRI synthesis with exceptional efficiency, it holds promise for improving diagnostic processes, accelerating neuroscientific inquiry, and deepening our understanding of the intricate relationships governing brain structure and function.

References

- [1] Benoit Anctil-Robitaille, Christian Desrosiers, and Herve Lombaert. Manifold-aware CycleGAN for high-resolution structural-to-DTI synthesis. In *Computational Diffusion MRI, Mathematics and visualization*, pages 213–224. Springer International Publishing, Cham, 2021.
- [2] Benoit Anctil-Robitaille, Antoine Théberge, Pierre-Marc Jodoin, Maxime Descoteaux, Christian Desrosiers, and Hervé Lombaert. Manifold-aware synthesis of high-resolution diffusion from structural imaging. *Front. Neuroimaging*, 1:930496, September 2022.
- [3] Vincent Bazinet, Reinder Vos de Wael, Patric Hagmann, Boris C Bernhardt, and Bratislav Mistic. Multiscale communication in cortico-cortical networks. *NeuroImage*, 243:118546, 2021.
- [4] Richard F Betzel and Danielle S Bassett. Multi-scale brain networks. *Neuroimage*, 160:73–83, 2017.
- [5] Hongjie Cai, Aojie Li, Guangjun Yu, Xiujun Yang, and Manhua Liu. Brain age prediction in developing childhood with multimodal magnetic resonance images. *Neuroinformatics*, 21(1):5–19, 2023.

- [6] Betty Jo Casey, Tariq Cannonier, May I Conley, Alexandra O Cohen, Deanna M Barch, Mary M Heitzeg, Mary E Soules, Theresa Teslovich, Danielle V Dellarco, Hugh Garavan, et al. The adolescent brain cognitive development (ab cd) study: imaging acquisition across 21 sites. *Developmental cognitive neuroscience*, 32:43–54, 2018.
- [7] Karissa Chan, Pejman Jabejdar Maralani, Alan R Moody, and April Khademi. Synthesis of diffusion-weighted MRI scalar maps from FLAIR volumes using generative adversarial networks. *Front. Neuroinform.*, 17:1197330, August 2023.
- [8] Yunpeng Chen, Haoqi Fan, Bing Xu, Zhicheng Yan, Yannis Kalantidis, Marcus Rohrbach, Shuicheng Yan, and Jiashi Feng. Drop an octave: Reducing spatial redundancy in convolutional neural networks with octave convolution. In *Proceedings of the IEEE/CVF international conference on computer vision*, pages 3435–3444, 2019.
- [9] Joseph Paul Cohen, Margaux Luck, and Sina Honari. Distribution matching losses can hallucinate features in medical image translation. In *Medical Image Computing and Computer Assisted Intervention–MICCAI 2018: 21st International Conference, Granada, Spain, September 16–20, 2018, Proceedings, Part I*, pages 529–536. Springer, 2018.
- [10] Gwenaëlle Douaud, Saâd Jbabdi, Timothy EJ Behrens, Ricarda A Menke, Achim Gass, Andreas U Monsch, Anil Rao, Brandon Whitcher, Gordon Kindlmann, Paul M Matthews, et al. Dti measures in crossing-fibre areas: increased diffusion anisotropy reveals early white matter alteration in mci and mild alzheimer’s disease. *Neuroimage*, 55(3):880–890, 2011.
- [11] Martin Dyrba, Michael Ewers, Martin Wegrzyn, Ingo Kilimann, Claudia Plant, Annahita Oswald, Thomas Meindl, Michela Pievani, Arun LW Bokde, Andreas Fellgiebel, et al. Combining dti and mri for the automated detection of alzheimer’s disease using a large european multicenter dataset. In *Multimodal Brain Image Analysis: Second International Workshop, MBIA 2012, Held in Conjunction with MICCAI 2012, Nice, France, October 1–5, 2012. Proceedings 2*, pages 18–28. Springer, 2012.
- [12] Egidio D’Angelo and Viktor Jirsa. The quest for multiscale brain modeling. *Trends in neurosciences*, 45(10):777–790, 2022.
- [13] Giovanni B Frisoni, Nick C Fox, Clifford R Jack Jr, Philip Scheltens, and Paul M Thompson. The clinical use of structural mri in alzheimer disease. *Nature Reviews Neurology*, 6(2):67–77, 2010.
- [14] Karl J Friston. Functional integration in the brain. *Human Brain Function 2nd edn Academic Press, San Diego*, pages 971–997, 2004.
- [15] Daniel T Ginat and Steven P Meyers. Intracranial lesions with high signal intensity on t1-weighted mr images: differential diagnosis. *Radiographics*, 32:499–516, 2012.
- [16] Ian Goodfellow, Jean Pouget-Abadie, Mehdi Mirza, Bing Xu, David Warde-Farley, Sherjil Ozair, Aaron Courville, and Yoshua Bengio. Generative adversarial networks. *Communications of the ACM*, 63(11):139–144, 2020.
- [17] Xuan Gu, Hans Knutsson, Markus Nilsson, and Anders Eklund. Generating diffusion mri scalar maps from t1 weighted images using generative adversarial networks. In *Image Analysis: 21st Scandinavian Conference, SCIA 2019, Norrköping, Sweden, June 11–13, 2019, Proceedings 21*, pages 489–498. Springer, 2019.
- [18] Xuan Gu, Hans Knutsson, Markus Nilsson, and Anders Eklund. Generating diffusion MRI scalar maps from T1 weighted images using generative adversarial networks. In *Image Analysis, Lecture notes in computer science*, pages 489–498. Springer International Publishing, Cham, 2019.
- [19] Donald J Hagler Jr, SeanN Hatton, M Daniela Cornejo, Carolina Makowski, Damien A Fair, Anthony Steven Dick, Matthew T Sutherland, BJ Casey, Deanna M Barch, Michael P Harms, et al. Image processing and analysis methods for the adolescent brain cognitive development study. *Neuroimage*, 202:116091, 2019.

- [20] Kevin D Harkins, Junzhong Xu, Adrienne N Dula, Ke Li, William M Valentine, Daniel F Gochberg, John C Gore, and Mark D Does. The microstructural correlates of t1 in white matter. *Magnetic resonance in medicine*, 75(3):1341–1345, 2016.
- [21] Lorna Harper, Giorgio G Fumagalli, Frederik Barkhof, Philip Scheltens, John T O’Brien, Femke Bouwman, Emma J Burton, Jonathan D Rohrer, Nick C Fox, Gerard R Ridgway, et al. Mri visual rating scales in the diagnosis of dementia: evaluation in 184 post-mortem confirmed cases. *Brain*, 139(4):1211–1225, 2016.
- [22] Phillip Isola, Jun-Yan Zhu, Tinghui Zhou, and Alexei A Efros. Image-to-image translation with conditional adversarial networks. In *Proceedings of the IEEE conference on computer vision and pattern recognition*, pages 1125–1134, 2017.
- [23] Justin Johnson, Alexandre Alahi, and Li Fei-Fei. Perceptual losses for real-time style transfer and super-resolution. In *Computer Vision—ECCV 2016: 14th European Conference, Amsterdam, The Netherlands, October 11-14, 2016, Proceedings, Part II 14*, pages 694–711. Springer, 2016.
- [24] Derek K Jones. The effect of gradient sampling schemes on measures derived from diffusion tensor mri: a monte carlo study. *Magnetic Resonance in Medicine: An Official Journal of the International Society for Magnetic Resonance in Medicine*, 51(4):807–815, 2004.
- [25] Derek K Jones, Thomas R Knösche, and Robert Turner. White matter integrity, fiber count, and other fallacies: the do’s and don’ts of diffusion mri. *Neuroimage*, 73:239–254, 2013.
- [26] Diederik P Kingma and Jimmy Ba. Adam: A method for stochastic optimization. *arXiv preprint arXiv:1412.6980*, 2014.
- [27] Manabu Kinoshita, Naoya Hashimoto, Tetsu Goto, Naoki Kagawa, Haruhiko Kishima, Shuichi Izumoto, Hisashi Tanaka, Norihiko Fujita, and Toshiki Yoshimine. Fractional anisotropy and tumor cell density of the tumor core show positive correlation in diffusion tensor magnetic resonance imaging of malignant brain tumors. *Neuroimage*, 43(1):29–35, 2008.
- [28] Marek Kubicki, Robert McCarley, Carl-Fredrik Westin, Hae-Jeong Park, Stephan Maier, Ron Kikinis, Ferenc A Jolesz, and Martha E Shenton. A review of diffusion tensor imaging studies in schizophrenia. *Journal of psychiatric research*, 41(1-2):15–30, 2007.
- [29] Joonwoo Kwon, Sooyoung Kim, Yuewei Lin, Shinjae Yoo, and Jiook Cha. Aesfa: An aesthetic feature-aware arbitrary neural style transfer. In *Proceedings of the AAAI Conference on Artificial Intelligence*, volume 38, pages 13310–13319, 2024.
- [30] Ya-di Li, Hui-jin He, Hai-bo Dong, Xiao-yuan Feng, Guo-ming Xie, and Ling-jun Zhang. Discriminative analysis of early-stage alzheimer’s disease and normal aging with automatic segmentation technique in subcortical gray matter structures: a multicenter in vivo mri volumetric and dti study. *Acta Radiologica*, 54(10):1191–1200, 2013.
- [31] Ulrike Lueken, Markus Muehlhan, Hans-Ulrich Wittchen, Thilo Kellermann, Isabelle Reinhardt, Carsten Konrad, Thomas Lang, André Wittmann, Andreas Ströhle, Alexander L Gerlach, et al. (don’t) panic in the scanner! how panic patients with agoraphobia experience a functional magnetic resonance imaging session. *European neuropsychopharmacology*, 21(7):516–525, 2011.
- [32] Chantel D Mayo, Erin L Mazerolle, Lesley Ritchie, John D Fisk, Jodie R Gawryluk, Alzheimer’s Disease Neuroimaging Initiative, et al. Longitudinal changes in microstructural white matter metrics in alzheimer’s disease. *NeuroImage: Clinical*, 13:330–338, 2017.
- [33] Kieran J Murphy and James A Brunberg. Adult claustrophobia, anxiety and sedation in mri. *Magnetic resonance imaging*, 15(1):51–54, 1997.
- [34] Augustus Odena, Vincent Dumoulin, and Chris Olah. Deconvolution and checkerboard artifacts. *Distill*, 1(10):e3, 2016.
- [35] Edward Ofori, Ofer Pasternak, Peggy J Planetta, Hong Li, Roxana G Burciu, Amy F Snyder, Song Lai, Michael S Okun, and David E Vaillancourt. Longitudinal changes in free-water within the substantia nigra of parkinson’s disease. *Brain*, 138(8):2322–2331, 2015.

- [36] Taesung Park, Jun-Yan Zhu, Oliver Wang, Jingwan Lu, Eli Shechtman, Alexei Efros, and Richard Zhang. Swapping autoencoder for deep image manipulation. *Advances in Neural Information Processing Systems*, 33:7198–7211, 2020.
- [37] Adam Paszke, Sam Gross, Francisco Massa, Adam Lerer, James Bradbury, Gregory Chanan, Trevor Killeen, Zeming Lin, Natalia Gimelshein, Luca Antiga, et al. Pytorch: An imperative style, high-performance deep learning library. *Advances in neural information processing systems*, 32, 2019.
- [38] Jiaolong Qin, Maobin Wei, Haiyan Liu, Jianhuai Chen, Rui Yan, Zhijian Yao, and Qing Lu. Altered anatomical patterns of depression in relation to antidepressant treatment: evidence from a pattern recognition analysis on the topological organization of brain networks. *Journal of affective disorders*, 180:129–137, 2015.
- [39] LR Ranzenberger and T Snyder. Diffusion tensor imaging. statpearls, 2022.
- [40] Mengwei Ren, Heejong Kim, Neel Dey, and Guido Gerig. Q-space conditioned translation networks for directional synthesis of diffusion weighted images from multi-modal structural MRI. *arXiv [eess.IV]*, June 2021.
- [41] R Rzedzian, P Mansfield, M Doyle, D Guilfoyle, B Chapman, RE Coupland, A Chrispin, and P Small. Real-time nuclear magnetic resonance clinical imaging in paediatrics. *The Lancet*, 322(8362):1281–1282, 1983.
- [42] Michael Schirner, Anthony Randal McIntosh, Viktor Jirsa, Gustavo Deco, and Petra Ritter. Inferring multi-scale neural mechanisms with brain network modelling. *elife*, 7:e28927, 2018.
- [43] Apoorva Sikka, Jitender Singh Virk, Deepti R Bathula, et al. Mri to pet cross-modality translation using globally and locally aware gan (gla-gan) for multi-modal diagnosis of alzheimer’s disease. *arXiv preprint arXiv:2108.02160*, 2021.
- [44] Karen Simonyan and Andrew Zisserman. Very deep convolutional networks for large-scale image recognition. *arXiv preprint arXiv:1409.1556*, 2014.
- [45] Qiyuan Tian, Berkin Bilgic, Qiuyun Fan, Congyu Liao, Chanon Ngamsombat, Yuxin Hu, Thomas Witzel, Kawin Setsompop, Jonathan R Polimeni, and Susie Y Huang. Deepdti: High-fidelity six-direction diffusion tensor imaging using deep learning. *NeuroImage*, 219:117017, 2020.
- [46] Jeffrey Tsao. Ultrafast imaging: principles, pitfalls, solutions, and applications. *Journal of Magnetic Resonance Imaging*, 32(2):252–266, 2010.
- [47] Lana Vasung, Elda Fischi-Gomez, and Petra S Hüppi. Multimodality evaluation of the pediatric brain: Dti and its competitors. *Pediatric radiology*, 43:60–68, 2013.
- [48] Qianye Yang, Nannan Li, Zixu Zhao, Xingyu Fan, Eric Chang, and Yan Xu. Mri cross-modality image-to-image translation. *Scientific Reports*, 10:3753, 02 2020.
- [49] Muhua Zheng, Antoine Allard, Patric Hagmann, Yasser Alemán-Gómez, and M Ángeles Serano. Geometric renormalization unravels self-similarity of the multiscale human connectome. *Proceedings of the National Academy of Sciences*, 117(33):20244–20253, 2020.
- [50] Zhong Zheng, Shirag Shemmassian, Christopher Wijekoon, Won Kim, Susan Y Bookheimer, and Nader Pouratian. Dti correlates of distinct cognitive impairments in parkinson’s disease. *Human brain mapping*, 35(4):1325–1333, 2014.
- [51] Jun-Yan Zhu, Taesung Park, Phillip Isola, and Alexei A Efros. Unpaired image-to-image translation using cycle-consistent adversarial networks. In *Proceedings of the IEEE international conference on computer vision*, pages 2223–2232, 2017.